Adsorption 7: 171–187, 2001

A Stefan-Maxwell Model of Single Pore Pressurization for Langmuir Adsorption of Gas Mixtures

J.A. DELGADO* AND A.E. RODRIGUES†
Laboratory of Separation and Reaction Engineering, Faculty of Engineering, University of Porto, Rua Dr. Roberto Frias s/n, 4200-465 Porto, Portugal
arodrig@fe.up.pt

Received September 7, 2000; Revised June 18, 2001; Accepted June 18, 2001

Abstract. A model based on the application of the Maxwell-Stefan approach has been used to describe the dynamics of intraparticle transport (pore diffusion, surface diffusion and convection) in a single pore during and after a pressurization process. The model was first compared with the model proposed by Taqvi and Levan (Adsorption, **2**, 299–309 (1996)) for a linear adsorption isotherm. The effect of several parameters (pressurization rate, adsorption capacity, bulk gas-phase mole fraction, adsorption affinity and pore radius) was studied, evaluating the relative importance of each mass-transport mechanism in different conditions. A binary mixture of an inert and an adsorbable component was considered first, extending the analysis of the pore radius effect to a ternary mixture. In general, surface diffusion is dominant with very low pore radius, whereas gas-phase fluxes dominate in a large pore. However, depending on the value of the bulk gas-phase mole fraction (which is related to the surface coverage level through the adsorption equilibrium isotherm), the equilibrium and rate parameters, and the surface to volume ratio, surface diffusion cannot be always neglected for large pores. More generally, system non-linearity can switch the dominant mechanism and create fronts.

Keywords: Maxwell-Stefan, pore diffusion, surface diffusion, convection, pressurization

Introduction

Pressure swing adsorption (PSA), widely used in process industries, provides an efficient way of using a selective sorbent for the separation of gas mixtures. The knowledge of the system behavior, needed for process design and optimization, can be obtained from simulation studies based on a mathematical model. In order to facilitate the analysis, it is useful to consider different levels of the system separately. One of the subsystems deserving special attention is a pore inside the adsorbent particle where mass transfer can occur according to several transport mechanisms; (i) diffusion in the fluid phase, usually called pore diffusion and including Knudsen and molecular diffusion, (ii) diffusion in the adsorbed phase (surface diffusion) and (iii) convective transport, caused by a total pressure gradient inside the pore.

Models of different complexity have been proposed in the literature for the description of intraparticle transport in PSA. Preliminary models neglected mass transfer resistances inside the particle, considering the mass and momentum balance in the interstitial gas in the bed only (Rodrigues et al., 1991). Lu et al. (1992a, 1992b) modeled intraparticle diffusion and convection by using Fick's and Darcy's law, respectively. They showed that intraparticle convection, which increases with the pore size of the adsorbent, lead in some cases to a better process performance. Taqvi and Levan (1996) studied the dynamics of intraparticle transport in a binary

*On leave from Department of Chemical Engineering, Universidad Complutense de Madrid, 28040 Madrid, Spain.
†To whom correspondence should be addressed.

system considering pore and surface diffusion and convection. The model proposed by these authors assumes constant Fickian diffusivities for pore and surface diffusion, absence of total pressure gradient in the pore and a linear adsorption isotherm.

For multicomponent systems, the dusty-gas model (Jackson, 1977; Mason and Malinauskas, 1983; Sotirchos, 1989) is one of the most rigorous descriptions of pore diffusion (including bulk and Knudsen diffusion) and convective transport. This model results from the application of the momentum-transfer approach, also called Maxwell-Stefan approach, to the gas-(pore wall molecules) mixture (Krishna and Wesselingh, 1997). Serbezov and Sotirchos (1997a, 1997b, 1998) applied the dusty gas model to intraparticle transport in a PSA system under isothermal and non-isothermal conditions. These authors did not consider surface diffusion in their work. As most models consider the formation of an adsorbed phase on the pore surface, surface diffusion may be a relevant transport mechanism if the mobility and the concentration of the sorbed species is high enough. Do and Do (1998) have used the Maxwell-Stefan approach to study the multicomponent transient diffusion in an activated carbon particle; however, surface diffusion flux was described by a Fickian expression proportional to the gradient of chemical potential. The results of this work show that surface transport is a relevant mechanism when the proposed model is validated with experimental data.

Krishna (1990, 1993a, 1993b) and Krishna and Wesselingh (1997) have extended the Maxwell-Stefan approach to describe intraparticle surface transport. Their formulation takes into account both the friction due to counterexchange of adsorbed molecules and the friction with the adsorbent.

The objectives of this paper are as follows;

(i) To develop a model for describing intraparticle transport of a multicomponent gaseous mixture in a single pore considering all posible mechanisms (pore and surface diffusion, convection) described by the Maxwell-Stefan approach.
(ii) Evaluate the effect of several parameters (pressurization rate, adsorption capacity, bulk gas-phase mole fraction, adsorption affinity and pore radius) on the relative importance of the different mechanisms during and after pressurization. A binary mixture of an inert carrier and an adsorbable compound is considered first.
(iii) To simulate the dynamics of the system in a large pore and a micropore considering a ternary mixture (one inert, two adsorbables of different affinity) in order to assess the differences in the profiles of partial pressure and fluxes for each component.

Model Description

A cylindrical pore exposed to the bulk fluid ($z = 0$) and closed at the other end ($z = L$, L being the pore length) is considered. The following assumptions are made in writing the mass balance equations:

1. The gas phase is ideal and the system is isothermal.
2. There are no radial concentration gradients.
3. Local equilibrium holds at any position in the pore at the gas-wall interface.
4. The adsorption equilibrium for the mixture can be described with the extended Langmuir isotherm.
5. Pore diffusion and convection are described with the Maxwell-Stefan approach.
6. Surface diffusion is described with the Maxwell-Stephan approach, assuming that Maxwell-Stefan diffusivities are independent of surface coverage and that countersorption diffusivities can be estimated with the Vignes relationship (Krishna and Wesselingh, 1997).

Molar Fluxes

The following nomenclature is used to distinguish the flux mechanisms; N_{dif} represents the diffusion flux resulting from partial pressure gradients (bulk and Knudsen diffusion); N_{vis} is the viscous flux due to total pressure gradient (convection) and N_{sur} is the flux driven by surface concentration gradients (surface diffusion). The letter N indicates molar flux with respect to a stationary cross-sectional surface. As the model is intended to hold for a multicomponent mixture (n components), matrix notation is convenient. Matrices are denoted with bold letters. From the Maxwell-Stefan approach, the following expressions are obtained for the vectors $\mathbf{N}_{\text{dif}}$ and $\mathbf{N}_{\text{vis}}$ ($n \times 1$) (Krishna, 1993b; Krishna and Wesselingh, 1997):

$$\mathbf{N}_{\text{dif}} = -\frac{1}{RT}\mathbf{B}^{-1}\frac{\partial \mathbf{p}}{\partial z} \tag{1}$$

$$\mathbf{N}_{\text{vis}} = -\frac{B_0}{\mu_{\text{m}} RT}\frac{\partial P}{\partial z}\mathbf{B}^{-1}\,\mathbf{\Lambda}\,\mathbf{p} \tag{2}$$

The parameter B_0 is the viscous flow parameter or permeability ($r^2/8$ for a cylindrical pore, r being the pore

radius). The parameter μ_m is the viscosity of the mixture, and for gases at moderate pressure it is adequately calculated from the semiempirical formula of Wilke et al. (Bird et al., 1960). The matrices $\mathbf{B}$ and $\mathbf{\Lambda}$ $(n \times n)$ are function of binary diffusivities (D_{ij}), Knudsen diffusivities ($D_{K,i}$) and mole fractions (y_i) as follows:

$$\mathbf{B} = \begin{cases} \dfrac{1}{D_{K,i}} + \displaystyle\sum_{\substack{j=1 \\ j\neq i}}^{n} \frac{y_j}{D_{ij}} & \text{for } i = j \\ -\dfrac{y_i}{D_{ij}} & \text{for } i \neq j \end{cases} \tag{3}$$

$$\mathbf{\Lambda} = \begin{cases} \dfrac{1}{D_{K,i}} & \text{for } i = j \\ 0 & \text{for } i \neq j \end{cases} \tag{4}$$

The binary diffusivities in Eq. (3) are functions of the total pressure and temperature according to Eq. (5)

$$D_{ij} = D_{ij}^{0}\left(\frac{P_0}{P}\right)\left(\frac{T}{T_0}\right)^{1.75} \tag{5}$$

where P_0 and T_0 are some reference pressure and temperature, respectively. The Knudsen diffusivities are

$$D_{K,i} = \frac{2r}{3}\sqrt{\frac{8RT}{\pi M_i}} \tag{6}$$

where M_i is the molecular weight of component i. The total flux in the gas phase results from the sum of $\mathbf{N}_{dif}$ and $\mathbf{N}_{vis}$ (Eqs. (1) and (2)). For the case of a pure gas, the resulting expression for the total gaseous flux agrees with the equation proposed by Mason and Malinauskas (1983) in this limiting case ($N_{dif} + N_{vis} = -1/RT\,(D_K + B_0 P/\mu)\partial P/\partial z$), which includes Knudsen and convective fluxes, the latter being predominant for large pores.

The expression for $\mathbf{N}_{sur}$ is derived from the equation proposed by Krishna and Wessenlingh (1997), adapted to a cylindrical pore and allowing for different saturation capacities of the components (Kapteijn et al., 1995);

$$\mathbf{N}_{sur} = -\frac{2}{r}\mathbf{n}_{sat}\mathbf{B}_s^{-1}\mathbf{\Gamma}\frac{\partial \boldsymbol{\theta}}{\partial z} \tag{7}$$

The matrix $\mathbf{n}_{sat}$ is defined as follows

$$\mathbf{n}_{sat} = \begin{cases} n_{sat,i} & \text{for } i = j \\ 0 & \text{for } i \neq j \end{cases} \tag{8}$$

where $n_{sat,i}$ is the saturation capacity of the component i, in mol·cm^{-2}. The vector of fractional occupancies, $\boldsymbol{\theta}$, is formed by the elements $\theta_i = n_i/n_{sat,i}$, where n_i is the surface concentration of the component i, in mol·cm^{-2}. The matrix $\mathbf{B}_s$ is given below

$$\mathbf{B}_s = \begin{cases} \dfrac{1}{D_i^{MS}} + \displaystyle\sum_{\substack{j=1 \\ j\neq i}}^{n} \frac{\theta_j}{D_{ij}^{MS}} & \text{for } i = j \\ -\dfrac{\theta_i}{D_{ij}^{MS}} & \text{for } i \neq j \end{cases} \tag{9}$$

For the extended Langmuir isotherm

$$\theta_i = \frac{b_i p_i}{1 + \sum_{j=1}^{n} b_j p_j}; \quad p_i = \frac{1}{b_i}\frac{\theta_i}{1 - \sum_{j=1}^{n}\theta_j} \tag{10}$$

the matrix $\mathbf{\Gamma}$ is

$$\mathbf{\Gamma} = \begin{cases} 1 + \dfrac{\theta_i}{1 - \sum_{j=1}^{n}\theta_j} & \text{for } i = j \\ \dfrac{\theta_i}{1 - \sum_{j=1}^{n}\theta_j} & \text{for } i \neq j \end{cases} \tag{11}$$

The elements of the matrix $\mathbf{\Gamma}$ are called thermodynamic factors and are calculated as $\Gamma_{ij} = \theta_i(\partial \ln p_i)/\partial\theta_j$.

The parameter D_i^{MS}, the Maxwell-Stefan surface diffusivity of the component i represents the facility of exchange between the sorbed component i and the vacant sites. The parameter D_{ij}^{MS} represents the facility for counter-exchange at an adsorption site when the sorbed species j is replaced by the species i. It is estimated with the Vignes relationship (Krishna and Wesselingh, 1997);

$$D_{ij}^{MS} = \left(D_i^{MS}\right)^{\frac{\theta_i}{\theta_i+\theta_j}}\left(D_j^{MS}\right)^{\frac{\theta_j}{\theta_i+\theta_j}} \tag{12}$$

Mass Balance Equation

The mass balance in a differential volume element of the pore with length dz is expressed as follows

$$P_a\frac{\partial \mathbf{n}}{\partial t} + \frac{A_a}{RT}\frac{\partial \mathbf{p}}{\partial t} = -A_a\left(\frac{\partial \mathbf{N}_{dif}}{\partial z} + \frac{\partial \mathbf{N}_{vis}}{\partial z} + \frac{\partial \mathbf{N}_{sur}}{\partial z}\right) = -A_a\left(\frac{\partial \mathbf{N}_{TOTAL}}{\partial z}\right) \tag{13}$$

where P_a and A_a are the perimeter and cross-sectional area of the pore, respectively. Using the equilibrium

condition, the partial pressure vector is eliminated from Eq. (13) leading to

$$\left[P_a \mathbf{n}_{\text{sat}} + \frac{A_a}{RT}\mathbf{J}(\boldsymbol{\theta})\right]\frac{\partial \boldsymbol{\theta}}{\partial t} = -A_a\left(\frac{\partial \mathbf{N}_{\text{TOTAL}}}{\partial z}\right) \quad (14)$$

where $\mathbf{J}(\boldsymbol{\theta})$ is the Jacobian of the vector $\mathbf{p}$ vs. the fractional occupancy vector $\boldsymbol{\theta}$. Introducing a dimensionless axial coordinate, $x = z/L$,

$$\frac{\partial \boldsymbol{\theta}}{\partial t} = \left(\frac{-A_a}{L}\right)\left[P_a \mathbf{n}_{\text{sat}} + \frac{A_a}{RT}\mathbf{J}(\boldsymbol{\theta})\right]^{-1}\left(\frac{\partial \mathbf{N}_{\text{TOTAL}}}{\partial x}\right) \quad (15)$$

Initial and Boundary Conditions

We assume that the pore is initially in equilibrium with the gas phase at a given pressure $P_{\text{l}} = 1$ atm. The pore is then pressurized to $P_{\text{h}} = 5$ atm at constant pressurization rate. The initial condition is

$$\mathbf{p} = \mathbf{p}^{\text{init}} \quad t = 0 \quad \forall x \quad (16)$$

where $p_i^{\text{init}} = P_{\text{l}} y_i^{\text{init}}$, y_i^{init} being the initial mole fraction of component i. The following expression has been used to calculate the evolution of partial pressures of each component at $x = 0$ (boundary condition)

$$\begin{aligned} p_i|_{x=0} &= p_i^{\text{init}} + \left(p_i^{\text{fl}} - p_i^{\text{init}}\right)[1 - \exp(-kt)] \\ &\quad + \left(p_i^{\text{fh}} - p_i^{\text{fl}}\right)\frac{t}{t_{\text{pres}}} \quad 0 < t \le t_{\text{pres}} \quad (17) \\ p_i|_{x=0} &= p_i^{\text{fh}} \quad t > t_{\text{pres}} \end{aligned}$$

where $p_i^{\text{fl}} = P_{\text{l}} y_i^{\text{f}}$, $p_i^{\text{fh}} = P_{\text{h}} y_i^{\text{f}}$, y_i^{f} being the mole fraction of the component i in the feed, and t_{pres} is the pressurization time. The parameter k is used to account for the change of composition at the pore mouth occurring when $y_i^{\text{f}} \neq y_i^{\text{init}}$. The value of k must be high enough for the partial pressures to be continuous at $t = t_{\text{pres}}$. Two pressurization times have been considered in this work, 1 and 4 seconds, in order to study the effect of the pressurization rate. These values are reasonable for a PSA process (Taqvi and LeVan, 1996). Accordingly, the value of k has been set to 100 s^{-1}, which is high enough to ensure the continuity of Eq. (17). Since the model equationsare solved for $\boldsymbol{\theta}$ instead of $\mathbf{p}$, the equilibrium condition is used to obtain the initial value of $\boldsymbol{\theta}$ at every point and its evolution at $x = 0$. The boundary conditions at the closed end of the pore ($x = 1$) are

$$\frac{\partial \mathbf{p}}{\partial x} = 0 \qquad \frac{\partial \boldsymbol{\theta}}{\partial x} = 0 \qquad x = 1 \quad (18)$$

Numerical Procedure

The model is solved numerically using the PDECOL package (Madsen and Sincovec, 1979), which uses orthogonal collocation on finite elements (OCFE) technique for the discretization of the spatial variable x. The collocation method reduces the PDE system for n components to an initial-value ODE system, which is integrated by a Gear-type solver. Polynomials of Dth order are used to compute the approximate solution. The spatial coordinate is divided into N intervals, resulting in $N + 1$ breakpoints. C continuity conditions are imposed on the polynomial pieces across all of the interior breakpoints, the collocation procedure yielding a semidiscrete system of $n[(D + 1)N - C(N - 1)]$ time dependent ordinary differential equations, including the boundary conditions differentiated with respect to time. In this work, $C = 2$, $D = 3$ and $N = 100$ were used.

Simulation Results and Discussion

Binary Mixtures

Comparison With Literature Results. The model was compared with the model studied by Taqvi and LeVan (1996) at the same conditions. The system studied by these authors consists of a cylindrical pore with adsorptive walls which is pressurized with a mixture of an adsorbable component A and an inert carrier B. The model is developed assuming constant Fickian pore and surface diffusivities, absence of total pressure gradients, and a linear isotherm. It is also assumed that the pore is large enough for Knudsen diffusion to be neglected (e.g., larger than 10^{-5} cm at 1 atm) and to do the comparison we replaced the Langmuir isotherm in our model by a linear isotherm ($n_{\text{A}} = k_{\text{A}}(p_{\text{A}}/RT)$). Table 1 shows the values of the parameters used in the simulation. The following parameters were defined, in order to do the comparison with the same dimensionless variables:

Table 1. Model parameter values for comparison with the Taqvi and Levan model (1996).

$T = T_0 = 283\,\text{K}$	$P_0 = 1\ \text{atm}$
$r = 8 \times 10^{-5}\ \text{cm}$	$k_\text{A} = 10r/2$
$L = 0.01\ \text{cm}$	$k_\text{B} \approx 0$
$D^0_\text{AB} = 0.1\ \text{cm}^2\cdot\text{s}^{-1}$	$D^\text{MS}_\text{A} = 10^{-3}\ \text{cm}^2\cdot\text{s}^{-1}$
$M_\text{A} = 30\,\text{g}\cdot\text{mol}^{-1}$	$D^\text{MS}_\text{B} = 10^{-3}\ \text{cm}^2\cdot\text{s}^{-1}$
$M_\text{B} = 28\ \text{g}\cdot\text{mol}^{-1}$	$t_\text{pres} = 4\ \text{s}$
$\mu_\text{A} = 0.87 \times 10^{-4}\ \text{g}\cdot\text{cm}^{-1}\cdot\text{s}^{-1}$	$y^\text{init}_\text{A} = y^\text{f}_\text{A} = 0.5$
$\mu_\text{B} = 1.7 \times 10^{-4}\ \text{g}\cdot\text{cm}^{-1}\cdot\text{s}^{-1}$	

Dimensionless time, $\tau = D^0_\text{AB} t/L^2$
Reference flux, $N_\text{A0} = P_0 D^0_\text{AB}/(RTL)$
Dimensionless molar average velocity, $v^* = B_0/\mu_m(\partial P/\partial z)L/D^0_\text{AB}$

In this case, pressurization is complete for $\tau = 4000$. Figure 1 shows the profiles of the dimensionless velocity, mole fraction, dimensionless convective flux and dimensionless pore diffusion flux at several times obtained with our model, compared with those obtained by Taqvi and LeVan. Surface flux data cannot be compared because they are not available in their work.

It is observed that both models predict similar profiles for the mentioned variables, but some differences are noticeable with regard to the evolution of the profiles and the absolute values of the variables. The molar average velocity follows the same trend qualitatively, the maximum velocity occurring at $\tau \approx 40$, and then falling rapidly before the pressurization is complete. In our model, the velocity is proportional to the total

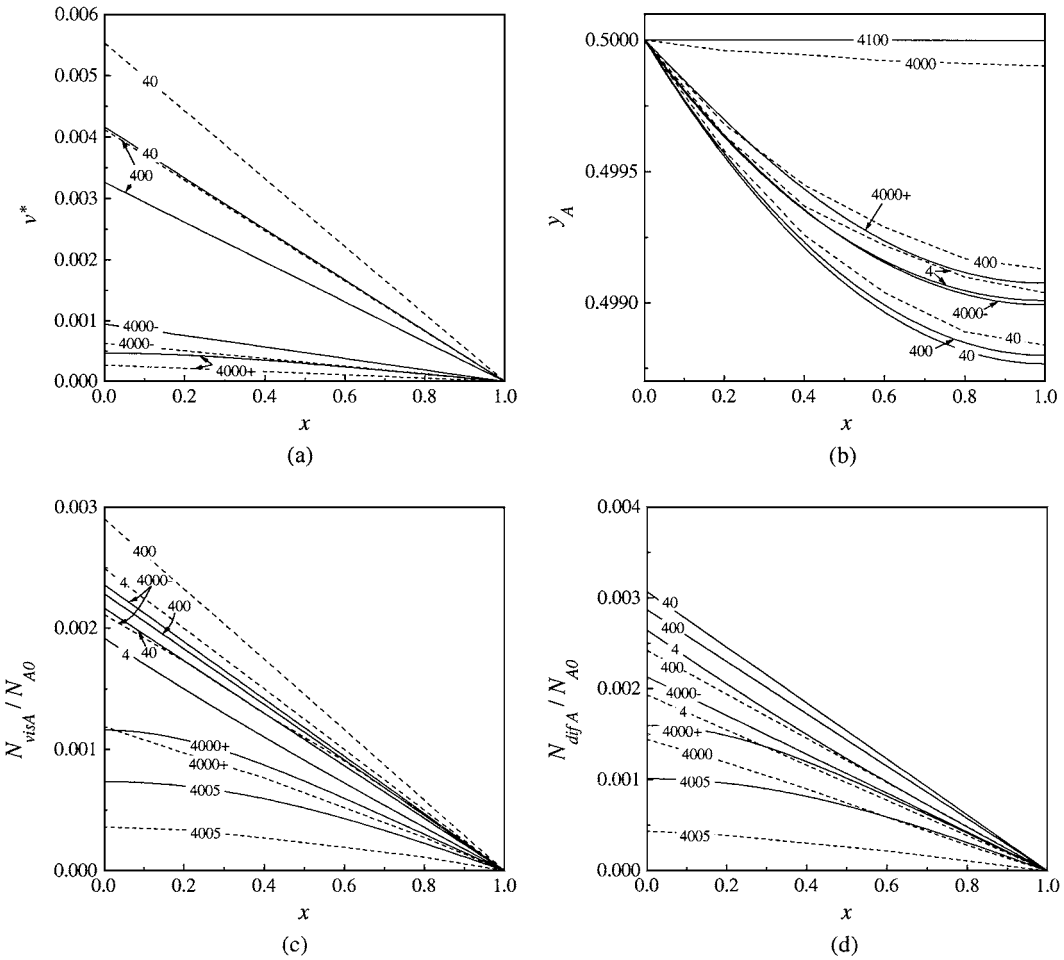

Figure 1. Simulated results for pore pressurization at various dimensionless times (τ) for a linear isotherm: (a) Velocity profiles; (b) Mole fraction profiles; (c) Convective flux profiles; (d) Pore diffusion profiles. Parameter values in Table 1. Dashed lines (- - -) are for Taqvi and LeVan (1996) model; full lines (—) are for our model.

pressure gradient, whereas the total pressure gradient is neglected in the other model. Taqvi and LeVan derived the following equation to calculate the velocity at x = 0;

$$\nu^*\big|_{x=0} = \frac{\left(k_A\frac{2}{r}+1\right)\frac{1}{P}\frac{dP}{d\tau} + k_A\frac{2}{r}\left(1-\frac{D_A^s}{D_{AB}}\right)\left(\frac{-\partial y_A}{\partial x}\Big|_{x=0}\right)}{k_A\frac{2}{r}\left(1-y_A\big|_{x=0}\right)+1} \tag{19}$$

where it can be seen that the decrease of velocity is caused by an increase of total pressure and a decrease of the mole fraction gradient. From a physical point of view, the different functional dependence of velocity in both models stems from the fact that the dissipation of energy caused by viscous friction is not considered in Eq. (19). This difference, in addition to other factors, such as the dependence of bulk diffusivity on total pressure, is responsible for the difference in flux and mole fraction profiles. The convective flux is smaller in our model at short times ($\tau < 400$, Fig. 1(c)) because the energy developed by pressurization is partially consumed by viscous friction, which is not considered in the other model. However, the viscous friction contributes to create the total pressure gradient, contributing to the diffusive flux because of the relationship between total and partial pressure gradients. Furthermore, the dependence of bulk diffusivity in total pressure also makes the mole fraction profiles more pronounced (Fig. 1(b)). As a result, the diffusive flux is higher in our model in this period. This situation changes from the pressurization time onwards. The mole fraction profiles are still significant at the pressurization time according to our model predictions, whereas they are very low in the other simulation. Accordingly, the fluxes also decrease faster in this period for the other model. In conclusion, it is observed that neglecting the total pressure gradient and the variation of bulk diffusivity when a pore is pressurized leads to higher convective flux, lower diffusive flux, and faster saturation of the pore, with respect to our model's predictions.

Effect of Pressurization Rate and Adsorptive Capacity. The effect of the pressurization rate in our system was analyzed by comparing the dependence with time and position of several variables for $t_{pres} = 1$ s and $t_{pres} = 4$ s. The pore is pressurized with a mixture nitrogen (1)-ethane (2) with the following conditions: $T = 303$ K, $L = 0.05$ cm, $r = 8.10^{-5}$ cm, $y_2^{init} = y_2^f = 0.5$. The other parameters used in the simulation are shown in Table 2. The variable used to measure the degree of saturation of the pore is the fractional uptake, which was defined as follows (Do and Do, 1998);

Table 2. Parameter values used in the simulations.[a,b]

$P_0 = 1$ atm	$T_0 = 303$ K
$D_{12}^0 = 0.1483$ cm^2·s^{-1}	$D_1^{MS} = 10^{-6}$ cm^2·s^{-1}
$D_{13}^0 = 0.1151$ cm^2·s^{-1}	$D_2^{MS} = 4\times10^{-6}$ cm^2·s^{-1}
$D_{23}^0 = 0.0798$ cm^2·s^{-1}	$D_3^{MS} = 10^{-6}$ cm^2·s^{-1}
$M_1 = 28$ g·mol^{-1}	$b_1 \approx 0$
$M_2 = 30$ g·mol^{-1}	$b_2 = 10.53$ atm^{-1}
$M_3 = 44$ g·mol^{-1}	$b_3 = 129$ atm^{-1}
$\mu_1 = 1.8\times10^{-4}$ g·cm^{-1}·s^{-1}	$n_{sat,1} \approx 0$
$\mu_2 = 0.925\times10^{-4}$ g·cm^{-1}·s^{-1}	$n_{sat,2} = 5.4\times10^{-7}$ mol·cm^{-2}
$\mu_3 = 0.8\times10^{-4}$ g·cm^{-1}·s^{-1}	$n_{sat,3} = 4.28\times10^{-7}$ mol·cm^{-2}

[a]Bulk diffusivities and viscosities taken from Do and Do (1998).
[b]Maxwell-Stefan surface diffusivities and equilibrium parameters of ethane and propane taken from Kapteijn et al. (1995). Adsorptive capacities in mol·cm^{-2} were estimated from the capacities in mol·(cc pore)$^{-1}$ for a pore of 8×10^{-5} cm. Nitrogen Maxwell-Stefan surface diffusivity was assumed.

$$F_i = \frac{\left(\frac{\bar{p}_i}{RT}+\frac{P_a}{A_a}n_{sat,i}\bar{\theta}_i\right)-\left(\frac{p_i^{init}}{RT}+\frac{P_a}{A_a}n_{sat,i}\theta_i^{init}\right)}{\left(\frac{p_i^{fh}}{RT}+\frac{P_a}{A_a}n_{sat,i}\theta_i^{fh}\right)-\left(\frac{p_i^{init}}{RT}+\frac{P_a}{A_a}n_{sat,i}\theta_i^{init}\right)} \tag{20}$$

where $\bar{p}_i$ and $\bar{\theta}_i$ are given below

$$\bar{p}_i = \int_0^1 p_i dx \quad \bar{\theta}_i = \int_0^1 \theta_i dx \tag{21}$$

The evolution of the fractional uptake assuming infinite rate of mass transfer inside the pore (equilibrium model) can be calculated by replacing $\bar{p}_i$ and $\bar{\theta}_i$ for $p_i|_{x=0}$ and $\theta_i|_{x=0}$ in Eq. (20).

Figure 2 shows the evolution of the ethane fractional uptake and the dependence with time and position of mole fraction, convective flux and pore diffusive flux, with two pressurization times (continuous lines, $t_{pres} = 4$ s, dashed lines, $t_{pres} = 1$ s, the numbers on the lines indicate t/t_{pres}). In Fig. 2(a) the fractional uptake obtained with the equilibrium model is included. This evolution is independent of pressurization rate if it is expressed as a function of t/t_{pres}. Taking as a reference

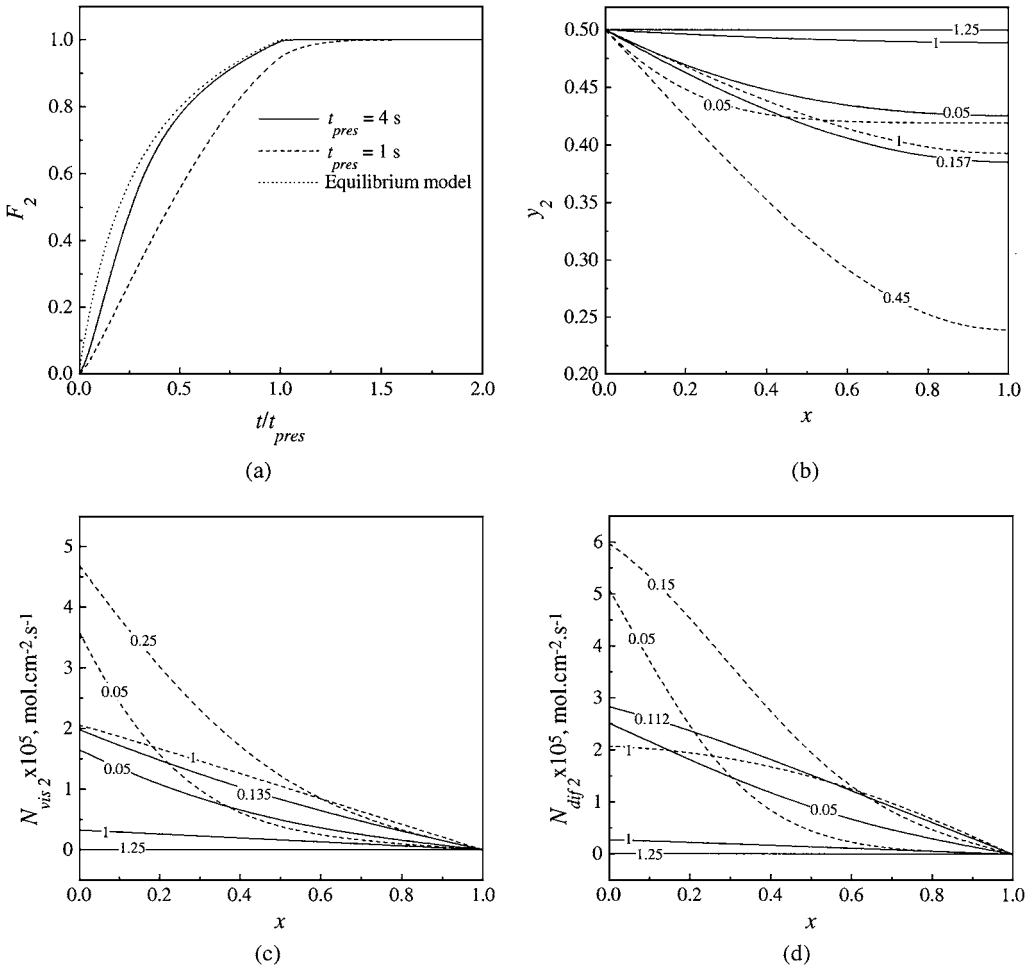

Figure 2. Effect of pressurization rate for a binary mixture nitrogen(1)-ethane(2) on: (a) Evolution of ethane fractional uptake; (b) Mole fraction profiles; (c) Convective flux profiles; (d) Pore diffusion flux profiles. Parameter values: $r = 8 \times 10^{-5}$ cm, $L = 0.05$ cm and $y_2^{\text{init}} = y_2^{\text{f}} = 0.5$. Full lines (—), $t_{\text{pres}} = 4$ s. Dashed lines (- - -), $t_{\text{pres}} = 1$ s. The numbers on lines denote t/t_{pres}.

the mole fraction at $x = 1$ and the fluxes at $x = 0$, the profiles corresponding to the time at which these variables are minimum (y_2) and maximum (N_{vis2}, N_{dif2}), are presented in Fig. 2. The profiles at $t/t_{\text{pres}} = 0.05$ and 1 are presented as well.

From Fig. 2(a), it is observed that the higher the pressurization rate, the lower the degree of saturation at the pressurization time. This result stems from the fact that an increase in the pressurization rate implies higher viscous friction, which causes stronger pressure and mole fraction gradients (Fig. 2(b)), also leading to a larger deviation from the equilibrium model.

Table 3 shows a comparison of the surface flux at $x = 0$ with the other fluxes at $t/t_{\text{pres}} = 0.05$, taken as a reference time. For this case, surface diffusion flux is small compared with other convective and diffusive fluxes. The results in Fig. 2(c) and (d) show that the pore diffusion and convective fluxes at $x = 0$ are of similar magnitude, although the diffusive flux is slightly higher. This similarity (with $y_2 = 0.5$) can be attributed to the fact that the total flux of the inert component is much lower than the total flux of ethane, so the system tends to the limiting case of diffusion through a stagnant gas (Taqvi and LeVan, 1996). This has been verified in Table 3. It occurs that the diffusive flux taking out nitrogen from the pore due to ethane adsorption compensates for the convective flux due to pressurization, so that the total flux of nitrogen is low.

In order to analyze the effect of the adsorptive capacity on the system behavior, the previous study was

Table 3. Fluxes (in mol·cm^{-2}·s^{-1}) at $x = 0$ and $t/t_{pres} = 0.05$ for a binary mixture 1-2 with $y_2^{init} = y_2^f = 0.5$.

t_{pres}, S	Adsorption	N_{vis2}	N_{dif2}	N_{sur2}	N_{TOTAL1}
1	Yes	3.58×10^{-5}	5.1×10^{-5}	6.60×10^{-7}	6.90×10^{-6}
1	No	3.00×10^{-6}	9.1×10^{-7}	0	4.02×10^{-6}
4	No	7.60×10^{-7}	2.5×10^{-7}	0	1.00×10^{-6}
4	Yes	1.65×10^{-5}	2.5×10^{-5}	3.30×10^{-7}	1.47×10^{-6}

1-nitrogen, 2-ethane.

repeated assuming that ethane is not adsorbed in the pore. A comparison of the fluxes in this case with the previous one at $x = 0$ and $t/t_{pres} = 0.05$ is shown in Table 3. It is observed that both convective and diffusive fluxes are reduced drastically, confirming the importance of adsorption induced convection, which has been reported elsewhere (Taqvi an LeVan, 1996). It is also observed that the ratio of convective to diffusive flux increases, since in absence of adsorption there are no mole fraction gradients if $y_i^{init} = y_i^f$. However, it is important to note that even though no adsorption occurs, the pore diffusion flux cannot be neglected (about 30% of convective flux), this flux being due only to the total pressure gradient in this case.

Effect of Bulk Mole Fraction and Adsorptive Affinity. The effect of bulk mole fraction was studied by varying the bulk mole fraction to 0.01 with respect to the previous case, for $t_{pres} = 4$ s. The effect of adsorptive affinity was analysed by comparing the results when nitrogen (1)-ethane (2) and nitrogen (1)-propane (3) mixtures are used. This comparison was performed for $y_{2,3}^{init} = y_{2,3}^f = 0.01$ and 0.5, because they correspond to different regions in the equilibrium isotherms. For $y_{2,3}^{init} = y_{2,3}^f = 0.01$, the slope of the adsorption isotherm is higher for propane than for ethane in the region under study, and for $y_{2,3}^{init} = y_{2,3}^f = 0.5$ is the reverse.

Figure 3(a) shows the evolution of fractional uptake of both adsorbates compared to that predicted by the equilibrium model, for the case $y_{2,3}^{init} = y_{2,3}^f = 0.01$. An important deviation from the equilibrium model is observed, which is reflected in a very high saturation time. This time is similar for ethane and propane because it depends on the available adsorptive capacity, estimated as $n_{sat}(\theta^{fh} - \theta^{fl})$, which is also similar for both compounds (about 1.3×10^{-7} mol·cm^{-2}). The high saturation time is a result of the low partial pressure of adsorbate in the feed, leading to a low velocity of propagation of the adsorption front with respect to the case with higher partial pressures. This velocity is inversely proportional to the slope of the adsorption isotherm, which has an dimensionless average value during the process of $(2/r)n_{sat}RT(\theta^{fh} - \theta^{fl})/(p^{fh} - p^{fl})$ As a Langmuir isotherm is used, at low pressures the velocity of the adsorption front is lower.

Figure 3(b) shows the evolution of the mole fraction profiles. It is observed that for $t \leq t_{pres}$ both the excess of ethane and propane with respect to the initial partial pressure is completely eliminated at $x > 0.5$. The remaining mole fraction stems from the initial partial pressure of adsorbate inside the pore ($t = 1$ s, $y|_{x=1} = 0.01$ atm / 2 atm; $t = 4$ s, $y|_{x=1} = 0.01$ atm/5 atm). It is also observed that the mole fraction gradient is stronger for propane than for ethane, which is due to its higher affinity. Figure 3(c) and (d) show the dependence with time and position of the surface diffusion and pore diffusion fluxes. In this case, surface flux is not negligible for ethane, unlike what was observed with higher bulk mole fraction. This result can be attributed to the low values of surface coverage occurring in this case with respect to previous other one. Let us assume that pore and surface diffusion can be described with Fickian expressions, so that pore diffusion flux is proportional to the partial pressure gradient and surface diffusion to the chemical potential gradient. Each flux is described with the following equations:

$$N_{dif} = -\frac{D_p^*}{RT}\frac{\partial p}{\partial z} \tag{22}$$

$$N_{sur} = -\frac{2}{r}n_{sat}\frac{D_s^{MS}}{(1-\theta)}\frac{\partial \theta}{\partial z} \tag{23}$$

where D_p^* is the effective pore diffusivity, equivalent to the bulk diffusivity in this case. The surface coverage gradient can be expressed as a function of partial pressure gradient by using the equilibrium condition

$$\frac{\partial \theta}{\partial z} = \frac{d\theta}{dp}\frac{\partial p}{\partial z} = \frac{1}{dp/d\theta}\frac{\partial p}{\partial z} = b(1-\theta)^2\frac{\partial p}{\partial z} \tag{24}$$

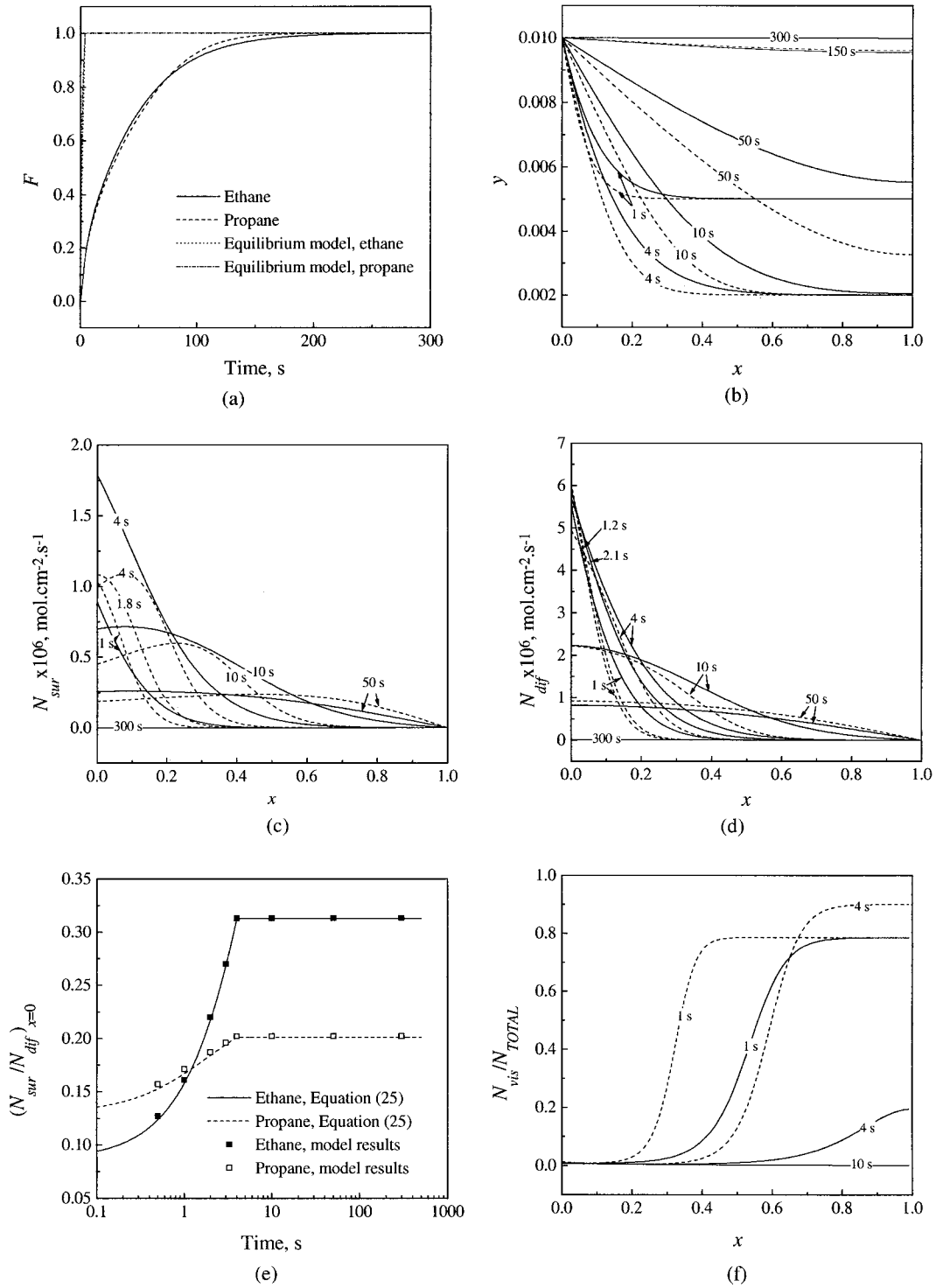

Figure 3. Pore transport dynamics for binary mixtures nitrogen(1)-ethane(2) and nitrogen(1)-propane(3). Full lines (—), ethane, dashed lines (- - -), propane: (a) Evolution of fractional uptake; (b) Mole fraction profiles; (c) Surface diffusion flux profiles; (d) Pore diffusion flux profiles; (e) Evolution of $(N_{\text{sur}}/N_{\text{dif}})_{x=0}$; (f) Variation of the relative importance of convective flux with time and position. Parameter values: $r = 8 \times 10^{-5}$ cm, $L = 0.05$ cm, $y_{2,3}^{\text{init}} = y_{2,3}^{\text{init}} = 0.01$ and $t_{\text{pres}} = 4$ s.

Introducing this equation in Eq. (23), the ratio of surface and pore diffusion fluxes is

$$\frac{N_{\text{sur}}}{N_{\text{dif}}} = \frac{\frac{2}{r} n_{\text{sat}} D_s^{\text{MS}} b(1-\theta)}{\frac{D_{\text{p}}^*}{RT}} \tag{25}$$

Therefore, when surface coverage tends to zero, surface contribution to pore transport is maximum, explaining the importance of surface diffusion in this case. The validity of Eq. (25) was verified by comparing the evolution of $(N_{\text{sur}}/N_{\text{dif}})_{x=0}$ calculated with Eq. (25) and that calculated with the whole model (Fig. 3(e)). The affinity has two opposite effects on this ratio; higher affinity means higher b but also lower surface diffusivity, so the stronger effect dominates.

With regard to the convective flux (Fig. 3(f)), it is observed that it is negligible at $x = 0$ during the pressurization, but it is predominant in the region not yet reached by the adsorption front. The zone where convective flux is dominating increases with the adsorptive affinity. This result is not obtained when a linear isotherm is used (Taqvi and LeVan, 1996), and indicates that the convective flux can be predominant even when a trace system is studied.

Table 4 shows a comparison of the fluxes of ethane and propane at $x = 0$ and $t = 0.2$ s when $y_{2,3}^{\text{init}} = y_{2,3}^{\text{f}} = 0.5$. At high surface coverage, the higher the affinity, the lower the available adsorptive capacity, which results in a behavior similar to that occurring when the adsorptive capacity is eliminated. It is observed that all the fluxes decrease significantly, and the ratio convective to diffusive flux increases. The ratio surface to pore diffusion flux is lower for propane than for ethane even if its equilibrium constant is 13 times higher and the bulk diffusivity is also lower, due to the lower surface diffusivity and the higher surface coverage (Eq. (25)).

Table 4. Fluxes (in mol·cm^{-2}·s^{-1}) at $x = 0$ and $t = 0.2$ s for binary mixtures 1-2, 1-3 with $y_{2,3}^{\text{init}} = y_{2,3}^{\text{f}} = 0.5$.

Component	N_{vis}	N_{dif}	N_{sur}
Ethane	1.65×10^{-5}	2.5×10^{-5}	3.30×10^{-7}
Propane	3.43×10^{-6}	3.55×10^{-6}	1.44×10^{-8}

1-nitrogen, 2-ethane, 3-propane.

Effect of the Pore Radius. The effect of the pore radius on the system dynamics was studied by simulating the process when a mixture ethane-nitrogen is pressurized with $t_{\text{pres}} = 4$ s, $y_2^{\text{init}} = y_2^{\text{f}} = 0.5$ and $r = 2 \times 10^{-7}$ cm. Figure 4(a) shows the evolution of fractional uptake. It is observed that the saturation time increases with respect to that obtained with $r = 8 \times 10^{-5}$ cm (Fig. 2(a)). This high saturation time is obtained because the total flux is not enough to provide all the ethane being adsorbed. This point is illustrated in Fig. 4(b), where it is observed that mole fraction gradients are important. Figure 4(c) also shows that the convective flux is not able to provide the nitrogen necessary to level the total pressure, leading to important total pressure gradients. As a result, for $t = t_{\text{pres}}$, the adsorption front has not arrived at the pore end and the mole fraction at $x = 1 (\sim 0.16)$ results from the initial partial pressure (0.5 atm) and the total pressure (3.1 atm). The minimum mole fraction at $x = 1$ occurs at $t > t_{\text{pres}}$ because nitrogen continues arriving at this position while the adsorption front has not arrived yet.

Figure 4(d) shows the dependence with time and position of the surface flux. In this case, N_{dif} and N_{vis} are not shown because N_{sur} is dominant. This is so because surface flux is proportional to $2/r$, thus being increased when r decreases, whereas N_{vis} is proportional to r^2 and N_{dif} to r (Knudsen flow with low r). This flux decreases rapidly with position in parallel with the partial pressure gradient (Fig. 4(c) for $t = 1$ s). However, it must be noted that for a short period ($0 < t < 1$ s), pore diffusion becomes about 25% of the total flux at those points where the adsorption front has not arrived. This result cannot be predicted with Eq. (25). It occurs that for this period the partial pressure gradient of ethane at these points is much lower than that of nitrogen (Fig. 4(c)), so that the cross-term $B_{21}{}^{-1} \partial p_1 / \partial x$ in Eq. (1) is not negligible. Thus, Eqs. (22) and (25) are not valid in this period.

Finally, in order to illustrate the effect of pore radius on the relevance of the different fluxes, the ratio $N_{(\text{flux type 2})}/(N_{\text{dif2}} + N_{\text{vis2}} + N_{\text{sur2}})(x = 0, t = 2 \text{ s})$ vs. r is shown in Fig. 4(e). It must be noted that these results are only valid for the conditions indicated. It is observed that at $r = 10^{-4}$ cm, the surface diffusion is already negligible and so is the total flux of nitrogen, so that the system tends to the limiting case of diffusion through a stagnant gas, as discussed before. The convective flux is less important the smaller the pore radius, but it is relevant with $r > 2 \times 10^{-6}$ cm. Surface diffusion dominates with $r < 2 \times 10^{-7}$ cm.

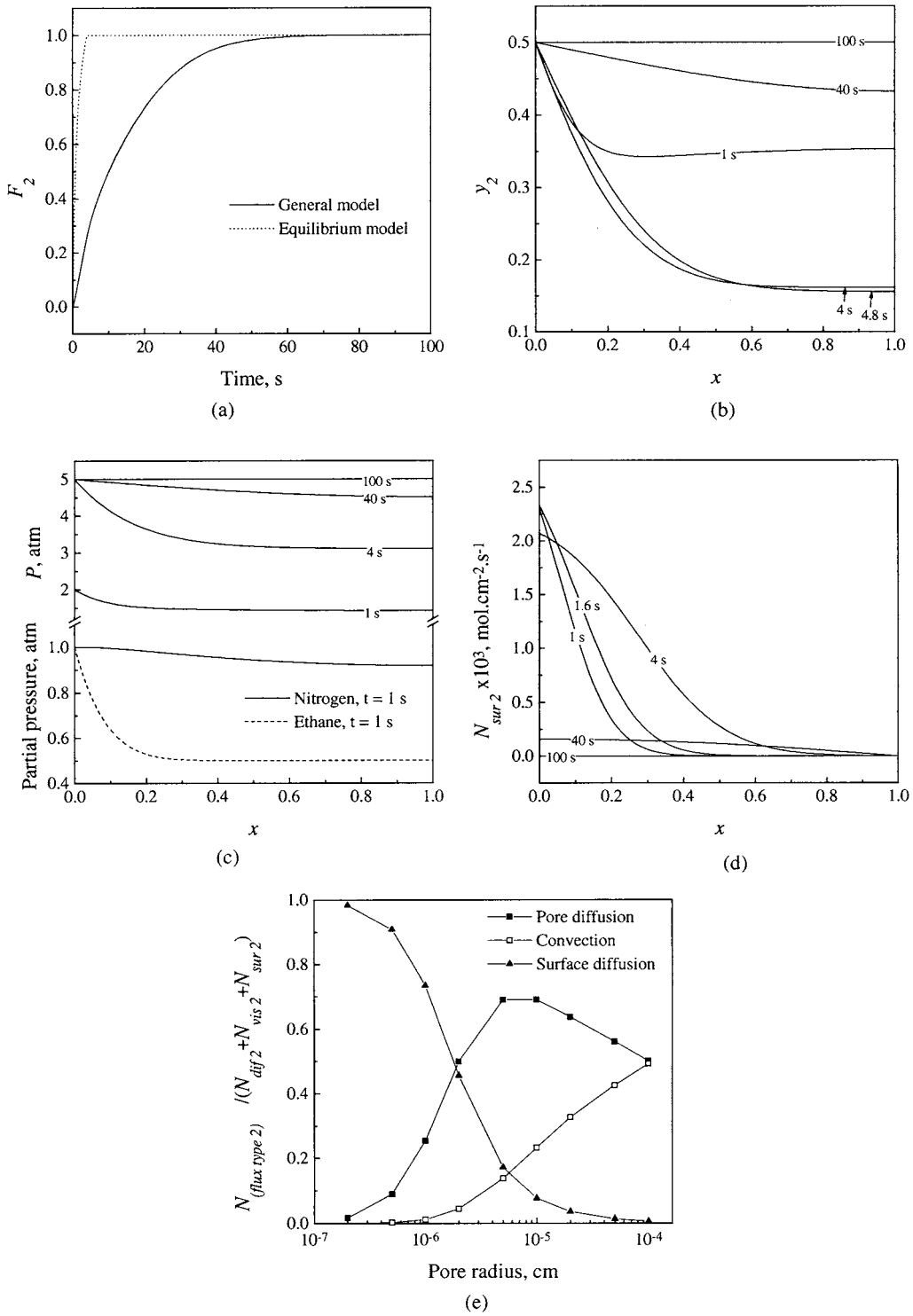

Figure 4. Pore transport dynamics for a binary mixture nitrogen(1)-ethane(2): (a) Evolution of fractional uptake, $r = 2 \times 10^{-7}$ cm; (b) Mole fraction profiles, $r = 2 \times 10^{-7}$ cm; (c) Total and partial pressure profiles, $r = 2 \times 10^{-7}$ cm; (d) Surface diffusion flux profiles, $r = 2 \times 10^{-7}$ cm; (e) Variation of the relative importance of different ethane fluxes with pore radius for $x = 0$ and $t = 2$ s. Other parameter values: $L = 0.05$ cm, $y_2^{\text{init}} = y_2^{\text{f}} = 0.5$ and $t_{\text{pres}} = 4$ s.

System Dynamics With a Ternary Mixture in a Large Pore

A simulation of the system dynamics for a ternary mixture (nitrogen-ethane-propane) in a large pore ($r = 8 \times 10^{-5}$ cm, 8000 Å) was carried out in order to analyze the behavior of each compound according to its affinity. The simulation parameters were $T = 303$ K, $L = 0.05$ cm, $p_1^{\text{init}} = 0.98$, $p_2^{\text{init}} = 0.01$ and $p_3^{\text{init}} = 0.01$ atm; $p_1^{\text{fl}} = p_2^{\text{fl}} = p_3^{\text{fl}} = (1/3)$ atm, $p_1^{\text{fh}} = p_2^{\text{fh}} = p_3^{\text{fh}} = (5/3)$ atm, and $t_{\text{pres}} = 4$ s. Figure 5(a) shows the evolution of fractional uptake for each compound. The curves for $r = 20$ Å are discussed later. It is observed that only the fractional uptake of propane increases in the normal fashion, whereas the one of nitrogen oscillates and that of ethane goes past the equilibrium value. This differences are caused by the displacement phenomena occurring in the pore surface, and it is necessary to consider the partial pressure profiles of the three compounds to explain this behavior, which are shown in Fig. 5(b) and (c). At short times, nitrogen goes out the pore due to the higher partial pressure inside the pore, which leads to negative values of F_1. This flux tends to level the partial pressure of nitrogen in the pore. However, as ethane and propane adsorption occurs, nitrogen fills the vacuum left by the adsorbable compounds, and enters the pore by convection against its partial pressure gradient, so that the positive gradient of nitrogen pressure is maintained for some time (Fig. 5(b)). As long as the adsorption fronts of ethane and propane do not arrive at $x = 1$, the partial pressure of nitrogen at this point increases with time, since it is the only component arriving at this position. In this period, F_1 increases with time, up to $t = 0.953$ s. However, when the faster adsorption front (ethane) arrives at $x = 1$ (about 0.8 s), ethane starts displacing nitrogen in the gas phase at the pore end, the former being displaced by propane in the adsorbed phase. This explains the sudden decrease in F_1 from 0.953 s to 1.293 s. Once the partial pressure gradient of nitrogen has almost disappeared at 1.293 s, nitrogen goes into the pore again driven by convection. The values of F_2 higher than unity are due to the fact that the adsorption front of ethane goes faster than that of propane, so that there are points where the surface coverage of ethane is much higher than its equilibrium value. At $t = 1.193$ s, the fractional occupancy of propane is significant on all pore surface, so that F_2 goes down to unity.

Figure 5(d)–(f) show the evolution of convective and pore diffusion flux profiles for the three compounds. The surface flux of ethane and propane are negligible in this case, an example of ethane and propane surface flux being shown in Fig. 5(e) (enhanced graph). This example is also shown to remark the fact that it is possible to obtain pore diffusion and surface fluxes of different sign when the Maxwell-Stephan approach is used to describe the surface flux, as it is the case in this example. The dragging effect of propane makes the surface flux of ethane positive, whereas the pore diffusion flux is negative. This is not possible when simple Fickian expressions are used, since they do not account for the influence of other component fluxes on the flux of one component.

Regarding the low values of surface flux, a simple expression like Eq. (25) cannot be obtained in this case, but it is reasonable to attribute this result to the effect of pore radius on the ratio $N_{\text{sur}}/N_{\text{dif}}$, which overcomes the influence of the other parameters. The effect of low surface coverage is only present at short times, disappearing when all the components are present at all positions ($t = 1.193$ s).

In Fig. 5(d), it is observed that the convective and diffusive flux profiles of nitrogen are almost symmetric, so the total flux is quite low compared with those of the other components. A similar result was obtained in the case dealing with a binary mixture nitrogen-ethane (0.5:0.5), and it is attributed to the higher capacity of the adsorbed phase in comparison with the gas phase, so that the total flux of inert compound is only that needed to level pressure. In contrast, the fluxes of adsorbable compounds must be enough to level their partial pressure and saturate the pore surface. It has been estimated that the amount of nitrogen, in mol, necessary to increase the pressure from 0.98 to (5/3) atm is 18 and 150 times lower than the amount of ethane and propane required to saturate the pore, respectively.

As for the fluxes of ethane and propane, it is observed that both convective and diffusive fluxes are important, although its ratio changes with time and position. The diffusive flux becomes dominant in the mass transfer zone of both components, until the adsorption fronts arrive at the pore end ($t < 1$ s). However, at $x = 0$ the convective flux is equal or higher than the diffusive one in this period. For higher times, diffusive flux is higher for both ethane and propane at all positions, which is attributed to the persistence of partial pressure gradients even at the pressurization time. In short, both convective and diffusive fluxes must be considered for a proper modeling of the system, and the formation of adsorption fronts and displacement

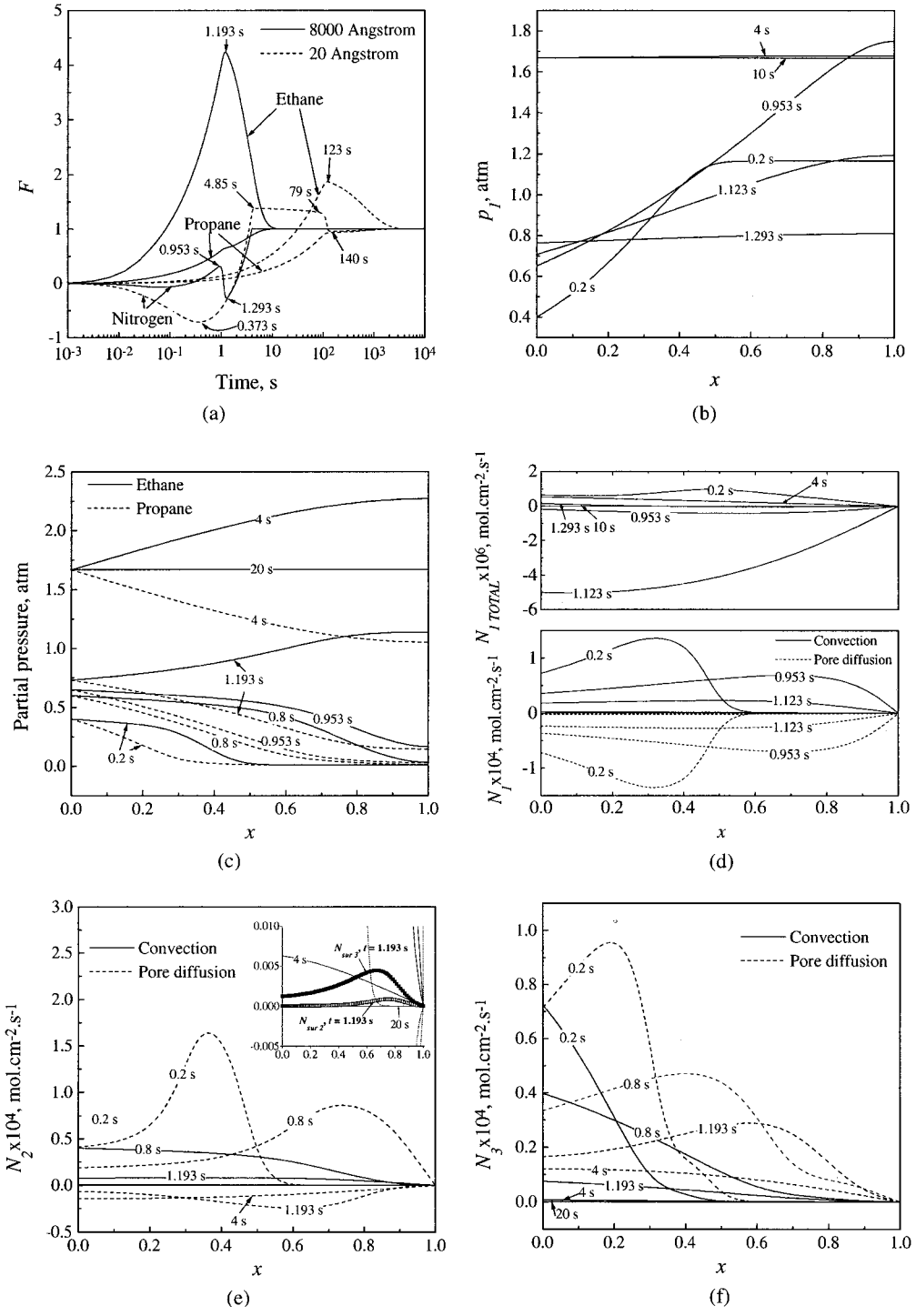

Figure 5. Pore transport dynamics for a ternary mixture nitrogen(1)-ethane(2)-propane(3): (a) Evolution of fractional uptake; (b) Nitrogen partial pressure profiles, $r = 8 \times 10^{-5}$ cm; (c) Ethane and propane partial pressure profiles, $r = 8 \times 10^{-5}$ cm; (d) Nitrogen flux profiles, $r = 8 \times 10^{-5}$ cm; (e) Ethane flux profiles, $r = 8 \times 10^{-5}$ cm. Enhanced graph including ethane and propane surface diffusion fluxes at $t = 1.193$ s; (f) Propane flux profiles, $r = 8 \times 10^{-5}$ cm. Other parameter values: $L = 0.05$ cm, $p_1^{\text{init}} = 0.98$ atm, $p_2^{\text{init}} = p_3^{\text{init}} = 0.01$ atm, $p_1^{\text{fl}} = p_2^{\text{fl}} = p_3^{\text{fl}} = (1/3)$ atm, $p_1^{\text{fh}} = p_2^{\text{fh}} = p_3^{\text{fh}} = (5/3)$ atm and $t_{\text{pres}} = 4$ s.

effects due to the use of a Langmuir isotherm makes its relative importance change with time and position significantly.

Effect of Pore Radius on System Dynamics With a Ternary Mixture. The previous simulation was performed for $r = 2 \times 10^{-7}$ cm, (20 Å), the other parameters being the same. The evolution of fractional uptake is shown in Fig. 5(a), and the evolution of total and partial pressures are shown in Fig. 6(a)–(c). The saturation time increases with respect to the previous case, due to two reasons; (i) the ratio pore capacity/pore cross-sectional area is higher, since it is inversely proportional to r and (ii) the permeability (B_0) and the effective pore diffusivity (Knudsen in this case) are much lower than with a large pore. Although surface flux is higher, being inversely proportional to r, it is not enough to overcome the previous effects. Figure 5(a) shows that the evolution of F_1 has changed significantly, whereas those of F_2 and F_3 have similar shape and just changed in magnitude. This is attributed to the strong decrease of gas-phase flux when r decreases, which affects more the non-adsorbed component. This change is also present in the partial pressure profiles (Figs. 5(b) and (c) and 6(b) and (c)), where it is observed that the nitrogen profiles show more important differences. The oscillation of F_1 is not observed in this case because the convective flux is less important now, so the nitrogen goes out of the pore by diffusion up to $t = 0.373$ s. When the positive partial pressure gradient has decreased at this

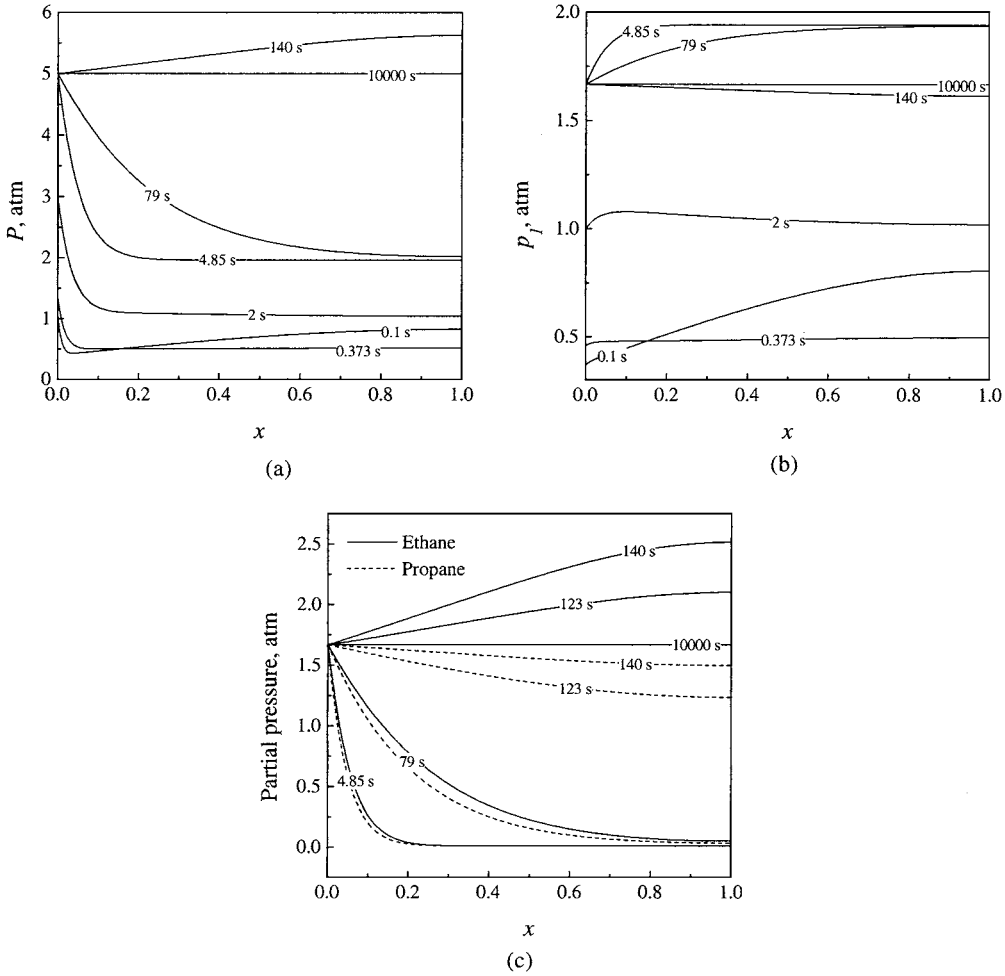

Figure 6. Pore transport dynamics for a ternary mixture nitrogen(1)-ethane(2)-propane(3): (a) Total pressure profiles; (b) Nitrogen partial pressure profiles; (c) Ethane and propane partial pressure profiles. Parameter values: $r = 2 \times 10^{-7}$ cm, $L = 0.05$ cm, $p_1^{\text{init}} = 0.98$ atm, $p_2^{\text{init}} = p_3^{\text{init}} = 0.01$ atm, $p_1^{\text{fl}} = p_2^{\text{fl}} = p_3^{\text{fl}} = (1/3)$ atm, $p_1^{\text{fh}} = p_2^{\text{fh}} = p_3^{\text{fh}} = (5/3)$ atm and $t_{\text{pres}} = 4$ s.

time, it enters by convection. The convective flux is favored by the partial pressure, which is is continuously increasing at $x = 0$. Nevertheless, the nitrogen convective flux is only important near the pore mouth, where the total pressure gradient is located (Fig. 6(a)). This leads to nitrogen partial pressure profiles with a maximum (Fig. 6(b), $t = 2$ s) because nitrogen accumulates in this zone, arriving at more internal points by diffusion. At $t = 4.85$ s, the internal partial pressure gradient disappears, and nitrogen goes out by diffusion against the total pressure gradient. At $t = 79$ s, the adsorption front of ethane arrives at $x = 1$ and ethane starts displacing nitrogen in the gas phase. Because of the low gas-phase flux, ethane cannot go out of the pore and accumulates at the pore end. As the fractional uptake is dominated by the concentration in the adsorbed phase, the maximum of F_2 at $t = 123$ s indicates a maximum in the average fractional occupancy of ethane. The accumulation of ethane in the gas phase continues up to 140 s, making total pressure increase above the external value, because the low gas-phase flux cannot level the gradient (Fig. 6(a)).

Table 5 shows the relative importance of the various fluxes for all components at two positions and two times. It is observed that the convective flux is not negligible for nitrogen at $x = 0$, despite the low permeability. This result can be attributed to the strong adsorption-induced convection occurring near the pore opening. The convective flux can be neglected for ethane and propane, but this not applies to the pore diffusion flux, which is significant for ethane with respect to the surface flux. Surface flux dominates for propane, which is the strongest adsorbed species. Therefore, it is concluded that the gas-phase flux with $r = 20$ Å is not negligible for the species with lower affinity, despite the increase of surface flux. This is attributable to the strong adsorption induced convection and to the displacement effects occurring in the system, which reduce the surface concentration of the species with intermediate affinity (ethane), increasing its partial pressure, thus reducing the relevance of its surface diffusion flux.

Table 5. Ratio between several fluxes at $x = 0$ and near the pore end at two times for a ternary mixture 1-2-3 with $r = 2 \times 10^{-7}$ cm.

	$t = 0.373$ s		$t = 4$ s	
	$x = 0$	$x \to 1$	$x = 0$	$x \to 1$
N_{dif1}/N_{vis1}	−0.9970	439.0	−0.792	120.0
N_{vis2}/N_{sur2}	0.0011	0.021	0.014	0.020
N_{dif2}/N_{sur2}	0.1570	0.194	0.499	0.185
N_{vis3}/N_{sur3}	0.0002	0.004	0.002	0.004
N_{dif3}/N_{sur3}	0.0230	0.037	0.078	0.035

1-nitrogen, 2-ethane, 3-propane.

Conclusions

A model based on the Maxwell-Stefan approach has been used to describe the dynamics of intraparticle transport (pore diffusion, surface diffusion and convection) in a single pore during and after a pressurization process. The model was first compared with the one proposed by Taqvi and Levan (1996) for a linear adsorption isotherm. The following conclusions can be drawn from this study:

(i) Neglecting the total pressure gradient and the variation of bulk diffusivity when a pore is pressurized leads to higher convective flux, lower diffusive flux and faster saturation of the pore, with respect to our model's predictions.
(ii) A higher pressurization rate leads to lower degree of saturation at the pressurization time. When the adsorptive capacity is eliminated, both convective and diffusive fluxes decrease, and the ratio of convective to diffusive flux increases. Total pressure gradient can contribute significantly to the pore diffusion flux for the case of constant gas-phase composition in the absence of adsorption.
(iii) The saturation time increases when the bulk mole fraction is decreased. Surface diffusion may be relevant with low bulk mole fraction in a large pore, because the contribution of surface diffusion to pore transport is higher the lower the surface coverage. In a trace system, convection is predominant in the zone not reached by the adsorption front.
(iv) The importance of gas-phase flux decreases when pore radius decreases, whereas that of surface diffusion flux increases. The combined effect of pore radius on the fluxes and the ratio pore capacity/pore cross-sectional area results in a higher saturation time when the pore radius is lower. Surface diffusion becomes dominant with very low pore radius values.
(v) The displacement phenomena occurring when a ternary mixture is considered makes the relative importance of each flux change with position and time. In a large pore, surface diffusion is negligible

in a bulk system, whereas both convective and diffusive fluxes are important. In a micropore, surface diffusion dominates for the strongest adsorbed species, whereas the gas-phase flux is relevant for the species with lower affinity.

Nomenclature

A_a Pore cross-sectional area, cm^2
b Adsorption affinity, atm^{-1}
$\mathbf{B}$ Matrix defined in Eq. (3), $cm^{-2}{\cdot}s$
B_0 Permeability, $cm^2{\cdot}s^{-1}$
$\mathbf{B}_s$ Matrix defined in Eq. (9), $cm^{-2}{\cdot}s$
D Diffusivity, $cm^2{\cdot}s^{-1}$
$\mathbf{J}$ Jacobian
k Parameter defined in Eq. (17), s^{-1}
L Pore length, cm
M Molecular weight, $g{\cdot}mol^{-1}$
n Number of components
$\mathbf{N}$ Vector of molar fluxes $(N_1, \ldots, N_n)$, $mol{\cdot}cm^{-2}{\cdot}s^{-1}$
$\mathbf{n}$ Vector of surface concentrations $(n_1, \ldots, n_n)$, $mol{\cdot}cm^{-2}$
P Total pressure, atm
$\mathbf{p}$ Vector of partial pressures $(p_1, \ldots, p_n)$, atm
P_a Pore perimeter, cm
R Ideal gas law constant, $J{\cdot}mol^{-1}{\cdot}K^{-1}$
r Pore radius, cm
T Temperature, K
t Time, s
v^* Dimensionless velocity
x Dimensionless axial coordinate, z/L
y Gas mole fraction
z Axial coordinate, cm

Greek Letters

$\mathbf{\Lambda}$ Matrix defined in Eq. (4), $cm^{-2}{\cdot}s$
$\mathbf{\Gamma}$ Matrix of thermodynamic factors, defined in Eq. (11)
$\boldsymbol{\theta}$ Vector of fractional occupancies $(\theta_1, \cdots, \theta_n)$, $\theta_i = n_i/n_{\mathrm{sat},i}$
μ Viscosity, $g{\cdot}cm^{-1}{\cdot}s^{-1}$
τ Dimensionless time, $D^0_{AB}t/L^2$

Subscripts

0 Reference value
A Adsorbable component
B Inert component
dif Pore diffusion
h High pressure
i, j Component numbers
K Knudsen
l Low pressure
m Mixture
pres Pressurization
sat Saturation
sur Surface
TOTAL Including the contributions of pore diffusion, convection and surface diffusion
vis Convection

Superscripts

$*$ Effective value or dimensionless velocity
0 Reference value
f Feed
h High pressure
init Initial value
l Low pressure
MS Maxwell-Stefan surface diffusivity

Acknowledgment

J.A. Delgado gratefully acknowledges financial support from Fundacion Flores-Valles-Universidad Complutense.

References

Bird, B., W. Stewart, and E. Lightfoot, *Transparent Phenomes*, J. Wiley, (Ed.), p. 24, New York, 1960.

Do, H.D. and D.D. Do, "Maxwell-Stefan Analysis of Multicomponent Transient Diffusion on a Capillary and Adsorption of Hydrocarbons in Activated Carbon Particle," *Chem. Engng. Sci.*, **53**, 1239–1252 (1998).

Jackson, R. *Transport in Porous Catalysis*, Elsevier, New York, 1977.

Kapteijn, F., W.J.W. Bakker, G. Zheng, J. Poppe, and J.A. Moulijn, "Permeation and Separation of Light Hydrocarbons Through a Silicalite-1 Membrane. Application of the Generalized Maxwell-Stefan Equations," *Chem. Engng. J.*, **57**, 145–153 (1995).

Krishna, R., "Multicomponent Surface Diffusion of Adsorbed Species: A Description Based on the Generalized Maxwell-Stefan Equations," *Chem. Engng. Sci.*, **45**, 1779–1791 (1990).

Krishna, R., "Problems and Pitfalls in the use of the Fick Formulation for Intraparticle Diffusion," *Chem. Engng. Sci.*, **48**, 845–861 (1993a).

Krishna, R., "A Unified Approach to the Modelling of Intraparticle Diffusion in Adsorption Processes," *Gas Separ. Purif.*, **7**, 91–104 (1993b).

Krishna, R. and J.A. Wesselingh, "The Maxwell-Stefan Approach to Mass Transfer," *Chem. Engng. Sci.*, **52**, 861–911 (1997).

Lu, Z., J.M. Loureiro, M.D. LeVan, and A.E. Rodrigues, "Intraparticle Convection Effect on Pressurization and Blowdown of Adsorbers," *AIChE J.*, **38**, 857–867 (1992a).

Lu, Z., J.M. Loureiro, M.D. LeVan, and A.E. Rodrigues, "Effect of Intraparticle Forced Convection on Gas Desorption from Fixed Beds Containing 'Large Pore' Adsorbents," *Ind. Engng. Chem. Res.*, **31**, 1530–1540 (1992b).

Madsen, N.K. and R.F. Sincovec, "PDECOL, General Collocation Software for Partial Differential Equations [D3]," *ACM Trans. Math. Software*, **5**, 326–351 (1979).

Mason, E.A. and A.P. Malinauskas, *Gas Transport in Porous Media: The Dusty-Gas Model*, Elsevier, New York, 1983.

Rodrigues, A.E., J.M. Loureiro, and M.D. LeVan, "Simulated Pressurization of Adsorption Beds," *Gas Sep. Purif.*, **5**, 115–124 (1991).

Serbezov, A. and S.V. Sotirchos, "Multicomponent Transport Effects in Sorbent Particles Under Pressure Swing Conditions," *Ind. Engng. Chem. Res.*, **36**, 3002–3012 (1997a).

Serbezov, A. and S.V. Sotirchos, "Mathematical Modeling of the Adsorptive Separation of Multicomponent Gaseous Mixtures," *Chem. Engng. Sci.*, **52**, 79–91 (1997b).

Serbezov, A. and S.V. Sotirchos, "Mathematical Modeling of Multicomponent Nonisothermal Adsorption in Sorbent Particles Under Pressure Swing Conditions," *Adsorption*, **4**, 93–111 (1998).

Sotirchos, S.V., "Multicomponent Diffusion and Convection in Capillary Structures," *AIChE J.*, **35**, 1953–1961 (1989).

Taqvi, S.M. and M.D. LeVan, "Role of Convection and Diffusion in a Single Pore With Adsorptive Walls," *Adsorption*, **2**, 299–309 (1996).